Journal of Solid State Chemistry **160,** 205–211 (2001)
doi:10.1006/jssc.2001.9224, available online at http://www.idealibrary.com IDEAL®

Pressure-Induced Phase Transitions in Cadmium Thiogallate $CdGa_2Se_4$

A. Grzechnik,*,[1] V. V. Ursaki,† K. Syassen,* I. Loa,* I. M. Tiginyanu,†,‡ and M. Hanfland§

*Max-Planck-Institut für Festkörperforschung, Heisenbergstrasse 1, D-70569 Stuttgart, Germany; †Institute of Applied Physics, Academy of Sciences of Moldova, 2028 Chisinau, Moldova; ‡Technical University of Moldova, 2004 Chisinau, Moldova; and §European Synchrotron Radiation Facility, B.P. 220, F-38000 Grenoble, France

Received February 5, 2001; in revised from April 18, 2001; accepted April 20, 2001; published online June 7, 2001

The high-pressure behavior of semiconducting cadmium thiogallate $CdGa_2Se_4$ with the defect chalcopyrite structure ($I\bar{4}$, $Z = 2$) is studied by *in situ* angle-dispersive synchrotron X-ray powder diffraction and optical reflectivity measurements in a diamond anvil cell at room temperature. At 21 GPa an order–disorder phase transition to the rock-salt structure ($F\bar{4}3m$, $Z = 4$) occurs. Upon decompression, the metallic NaCl-type polymorph transforms into zinc-blende ($Fm\bar{3}m$, $Z = 4$) at pressures of 7.5–4 GPa. The recovered metastable semiconducting material is of the zinc-blende type. © 2001 Academic Press

INTRODUCTION

The structure of chalcopyrite $CuFeS_2$ ($I\bar{4}2d$, $Z = 4$) is the simplest superstructure of the zinc-blende structure type ($F\bar{4}3m$, $Z = 4$) (1). It originates from a replacement of the Zn atoms by equal amounts of the Cu and Fe atoms in an ordered way, so that the unit cell is doubled along one of the [100] directions of zinc-blende. Cadmium thiogallates $CdGa_2X_4$ (X: S, Se) have a defect chalcopyrite structure ($I\bar{4}$, $Z = 2$), in which one of the cation sites is vacant (Fig. 1) (2, 3). Disorder of either the cations in chalcopyrite or the vacancies and one half of the cations in the corresponding defect structure leads to a famatinite (Cu_3SbS_4) type ($I\bar{4}2m$, $Z = 2$) present in zinc thiogallates $ZnGa_2X_4$ (4, 5). Complete disordering of the cations and vacancies yields the defect zinc-blende structure with fractional average occupation of cation sites.

Chalcopyrite-type materials have been extensively studied at high pressures using a variety of techniques. For instance, Raman spectroscopy (6), energy-dispersive X-ray powder diffraction (EDX) (7), and X-ray absorption (8) measurements show that $CuGaS_2$ transforms into the NaCl type ($Fm\bar{3}m$, $Z = 4$) at about 16 GPa. Based on the Raman scattering and EDX experiments, it was inferred that in $CuAlS_2$ and $CuAlSe_2$ the phase transitions from the chalcopyrite to the cubic structures (most probably of the rock-salt type) occur at about 16 and 12 GPa, respectively (9, 10). In all these cases, copper cations and either gallium or aluminum cations are considered to be fully disordered in the high-pressure NaCl-type phase. It should also be noted that there is no intermediate between this and the chalcopyrite structures. The situation encountered in the family of silver thiogallates is different. The sequence of pressure-induced phase transitions in $AgGaS_2$ with the ideal chalcopyrite structure toward disordered rock-salt involves two intermediate polymorphs (6, 7, 11). The first polymorph is of the monoclinically distorted (pseudotetragonal) chalcopyrite type (Cc, $Z = 4$). The second polymorph is the α-$NaFeO_2$ type ($R\bar{3}m$, $Z = 1$), a superstructure of the rock-salt type, with fully ordered Ag and Ga atoms. The first phase transition in $AgGaTe_2$ taking place at 3.1 GPa is from the chalcopyrite phase to the coexisting polymorph of the disordered zinc-blende type ($P\bar{4}$, $Z = 2$) and a second undetermined polymorph (12). The chalcopyrite phase disappears at 5.4 GPa. Two additional high-pressure phases occur at 8.5 GPa. One of them is assigned to the disordered NaCl type. The disordered zinc-blende type has also been considered as a high pressure structure of chalcopyrites (13, 14).

The high pressure behavior of the defect compounds is less known. Based on Raman scattering measurements, it is believed that the pressure-induced phase transitions in both cadmium and zinc thiogallates to the rock-salt type involve a defect zinc-blende polymorph (15). In the case of $CdGa_2Se_4$, it was argued that the formation of the disordered sixfold-coordinated phase at 15 GPa would proceed in two steps with defect famatinite and zinc-blende intermediates occurring at 5.5 GPa and 11.0 GPa, respectively. The recovered samples of $CdGa_2Se_4$ and $ZnGa_2Se_4$ are metastable high pressure rock-salt phases, while $CdGa_2S_4$ and $ZnGa_2S_4$ are partially amorphous.

In this study, we examine the high pressure behavior of cadmium selenogallate $CdGa_2Se_4$ using *in situ* synchrotron angle-dispersive X-ray powder diffraction and optical

[1] To whom correspondence should be addressed. E-mail: andrzej@servix.mpi-stuttgart.mpg.de.

0022-4596/01 $35.00

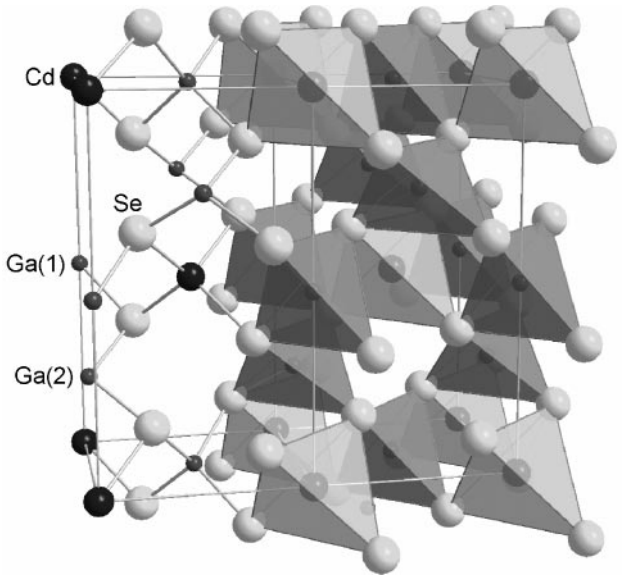

FIG. 1. Crystal structure of $CdGa_2Se_4$ at ambient conditions ($I\bar{4}$, $Z = 2$, $a = 5.743(2)$ Å, $c = 10.756(4)$ Å) (3). All atoms are labeled. The light and dark tetrahedra are around the Cd and Ga atoms, respectively.

reflectivity in a diamond anvil cell at room temperature. Materials derived from tetrahedrally coordinated zinc-blende type semiconductors, including defect variants, have promising optoelectronic properties at ambient conditions (16). High-pressure techniques offer possibilities to synthesize new metastable disordered compounds for which the optical properties would be altered. Our study of pressure-induced order–disorder phenomena in $CdGa_2Se_4$ could provide insights on a formation of metastable phases in zinc-blende derived materials.

EXPERIMENTAL

A single crystal of $CdGa_2Se_4$, grown by chemical vapor transport with iodine as a transport agent (3), was ground to a fine powder and subsequently loaded into a diamond anvil cell with a methanol–ethanol pressure medium. Although it solidifies around 7–8 GPa and afterward does not give fully hydrostatic conditions, this pressure medium was chosen to ensure a full comparison of the present X-ray diffraction results with the results of the previous Raman scattering study of the same material (15). Angle-dispersive powder X-ray diffractograms were measured on the ID9 beamline at the European Synchrotron Radiation Facility, Grenoble. Monochromatic radiation at a wavelength of 0.41416(1) Å was used for pattern collection on image plates. The images were integrated using the program FIT2D (17) to yield intensity versus 2θ diagrams. The instrumental resolution, i.e., the minimum full width at half maximum (FWHM) of diffraction peaks was 0.04°. To improve powder averaging, the DAC was rotated by $\pm 3°$. Optical reflectance spectra were recorded in the 0.6–4 eV range. In these experiments, the sample was in direct optical contact with one of the diamond anvils and the reflectance data reported below refer to the interface between diamond and sample. The spectra are corrected for absorption in the diamond window and reflection losses at the external diamond–air interface. Details are given elsewhere (18). The ruby luminescence method (19) was used for pressure calibration.

Full Rietveld refinements of X-ray patterns for defect chalcopyrite were carried out using the program GSAS (20). The refined parameters were: the fractional coordinates of Se, isotropic thermal parameters, Chebyshev polynomial background, Stephens profile function (21), an overall intensity scaling factor, and cell parameters. A preferred orientation correction was not considered. The Stephens function (21) was used in this work because it incorporates an anisotropic broadening of reflections due to strain, stacking faults, and shear stress that could develop under not purely hydrostatic conditions. Consequently, the systematic errors due to the nonhydrostatic effects inflicted on Rietveld refinements are minimized.

RESULTS AND DISCUSSION

X-Ray Diffraction

In the defect chalcopyrite structure of $CdGa_2Se_4$ (Fig. 1) all cations are at special Wyckoff positions ($I\bar{4}$, $Z = 2$)—Cd at $2a$ $(0, 0, 0)$, Ga(1) at $2b$ $(0, 0, 0.5)$, and Ga(2) at $2c$ $(0, 0.5, 0.25)$ (3). The ordered vacancy is at the $2d$ site (0, 0.5, 0.75). Each of the cations is tetrahedrally coordinated to selenium atoms at the $8g$ sites (x, y, z). The main feature of this structure is the angular distortion of the tetrahedra at both Ga positions. The tetrahedron around Ga(1) is elongated, while it is compressed around Ga(2). The distances between the Se atoms and vacancies are shorter than the Cd–Se bond length and both Ga–Se bond lengths.

Diffraction diagrams measured at different pressures and room temperature are shown in Fig. 2. At pressures up to about 20 GPa, all the diffraction peaks are due to the defect chalcopyrite structure. At 21 GPa, additional peaks appear indicating the onset of a phase transition. The new phase, showing only a few broad peaks, fully develops at higher pressures. Upon decompression, it is seen down to about 7.5 GPa, where a sluggish transition (about 3 GPa coexistence region) to another phase occurs. The pattern of the fully decompressed sample shows anomalously broadened reflections. It is clearly different from the patterns for the defect chalcopyrite and the high pressure phase formed above 21 GPa.

Selected patterns (at 5.5, 11.0, 15.0, and 18.1 GPa) of the defect chalcopyrite polymorph were refined with a Rietveld method (20) to obtain detailed information on the pressure evolution of structural parameters. The chosen

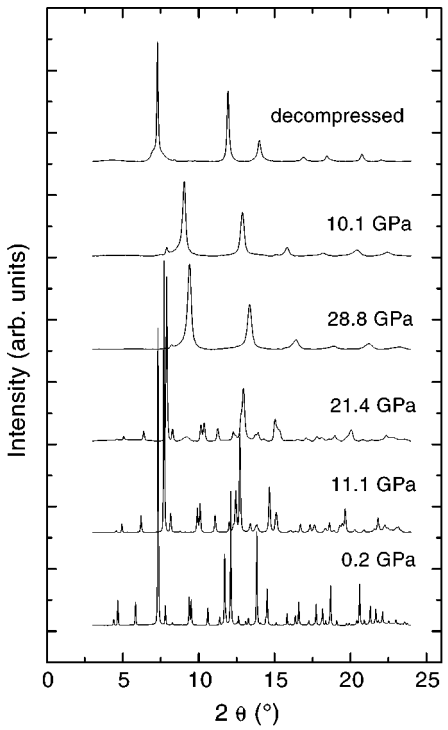

FIG. 2. Selected X-ray diffraction patterns of $CdGa_2Se_4$ at different pressures ($\lambda = 0.41416(1)$ Å). A smooth background arising mainly from Compton scattering in the diamond anvils is subtracted from all diffraction diagrams.

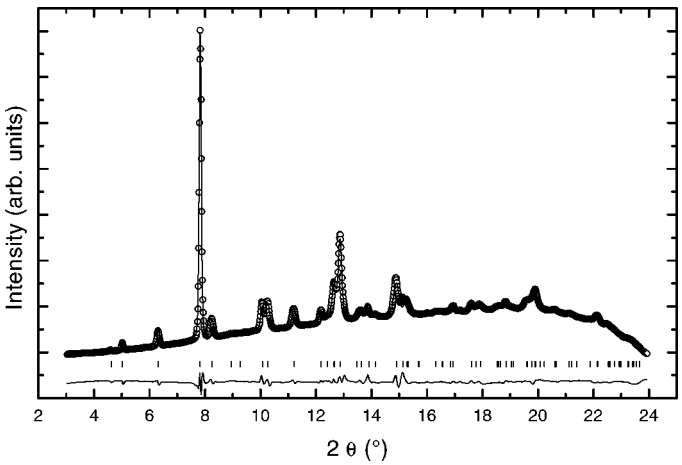

FIG. 3. Observed, calculated, and difference XRD profiles for $CdGa_2Se_4$ ($I\bar{4}$, $Z = 2$) at 18.1 GPa. Vertical markers indicate Bragg reflections ($\lambda = 0.41416(1)$ Å). The fitted standard R_{wp} and R_p factors are 1.8 and 1.2%, respectively, and χ^2 is 0.56. The corresponding R_{wp} and R_p factors without the background are 2.9 and 2.1%, respectively.

experimental patterns were for pressures that according to previous Raman scattering measurements (15) should display the phase transitions: defect chalcopyrite → defect famatinite → zinc-blende → rock-salt phase transitions were to take place according to the previous Raman scattering measurements. However, we find no indication for any structural change in $CdGa_2Se_4$ to about 21 GPa (see Fig. 1) and all the patterns up to this pressure are very well Rietveld refined with the defect chalcopyrite model (3). As an example, we show in Fig. 3, the result of the refinement for the pattern taken at 18.1 GPa. Corresponding parameters are given in Table 1.

The pressure dependence of structural parameters is illustrated in Fig. 4. The internal structural parameters being most sensitive to increasing pressure are the Ga(1)–Se–Ga(2) and Cd–Se–Ga(1) intertetrahedral angles and the angles in the CdS_4 and $Ga(2)Se_4$ tetrahedra. The changes in bond distances between the cations and the Se atoms are much smaller than the pressure-induced shortening of the distance between the anions and the ordered vacancy. All these observations indicate that anions move toward the empty site upon increasing pressure, while the tetrahedra enclosing the void are tilted. It should also be noticed that the c/a axial ratio increases. The change in the rate of increase of the c/a ratio with pressure near 7 GPa is not associated with any structural transformation, but could be related to the solidification of the pressure medium used (see the Experimental section). The parameter $\delta = 2\text{-}c/a$ is commonly used as a measure of a tetragonal distortion in the simple zinc-blende superstructures. Earlier it was shown that the order–disorder phase transitions in chalcopyrites at high temperatures and ambient pressure only take place when $\delta < 0.05$, while the compounds with $\delta < 0.05$ retain their defect chalcopyrite structure up to their melting points (22).

TABLE 1
Structural Data Obtained from a Full Rietveld Refinement (20) of the Pattern for $CdGa_2Se_4$ Collected at 18.1 GPa-$I\bar{4}$ ($Z = 2$), $a = 5.3167(2)$ Å, $c = 10.2858(6)$ Å, $V = 290.75(2)$ Å^3

Atom	Site	x	y	z
Cd	2*a*	0	0	0
Ga(1)	2*b*	0	0	$\frac{1}{2}$
Ga(2)	2*c*	0	$\frac{1}{2}$	$\frac{1}{4}$
Se	8*g*	0.2936(6)	0.229(1)	0.1448(3)
		Distances (Å)		
Cd–Se		2.477(4)	Ga(1)–Se	2.344(4)
Ga(2)–Se		2.384(4)	Vacancy (2*d*)–Se	1.964[a]
		Angles (°)		
Se–Cd–Se (4x)		111.2(1)	Se–Cd–Se′ (2x)	106.1(2)
Se–Ga(1)–Se (4x)		113.8(1)	Se–Ga(1)–Se′ (2x)	101.1(2)
Se–Ga(2)–Se (4x)		101.9(1)	Se–Ga(2)–Se′ (2x)	126.0(2)
Cd–Se–Ga(1)		102.4(1)	Cd–Se–Ga(2)	99.1(2)
Ga(1)–Se–Ga(2)		102.9(2)		

Note. Estimated standard deviations are given in parentheses.
[a] The vacancy in the defect chalcopyrite structure is located at the 2*d* Wyckoff site ($0, \frac{1}{2}, \frac{3}{4}$).

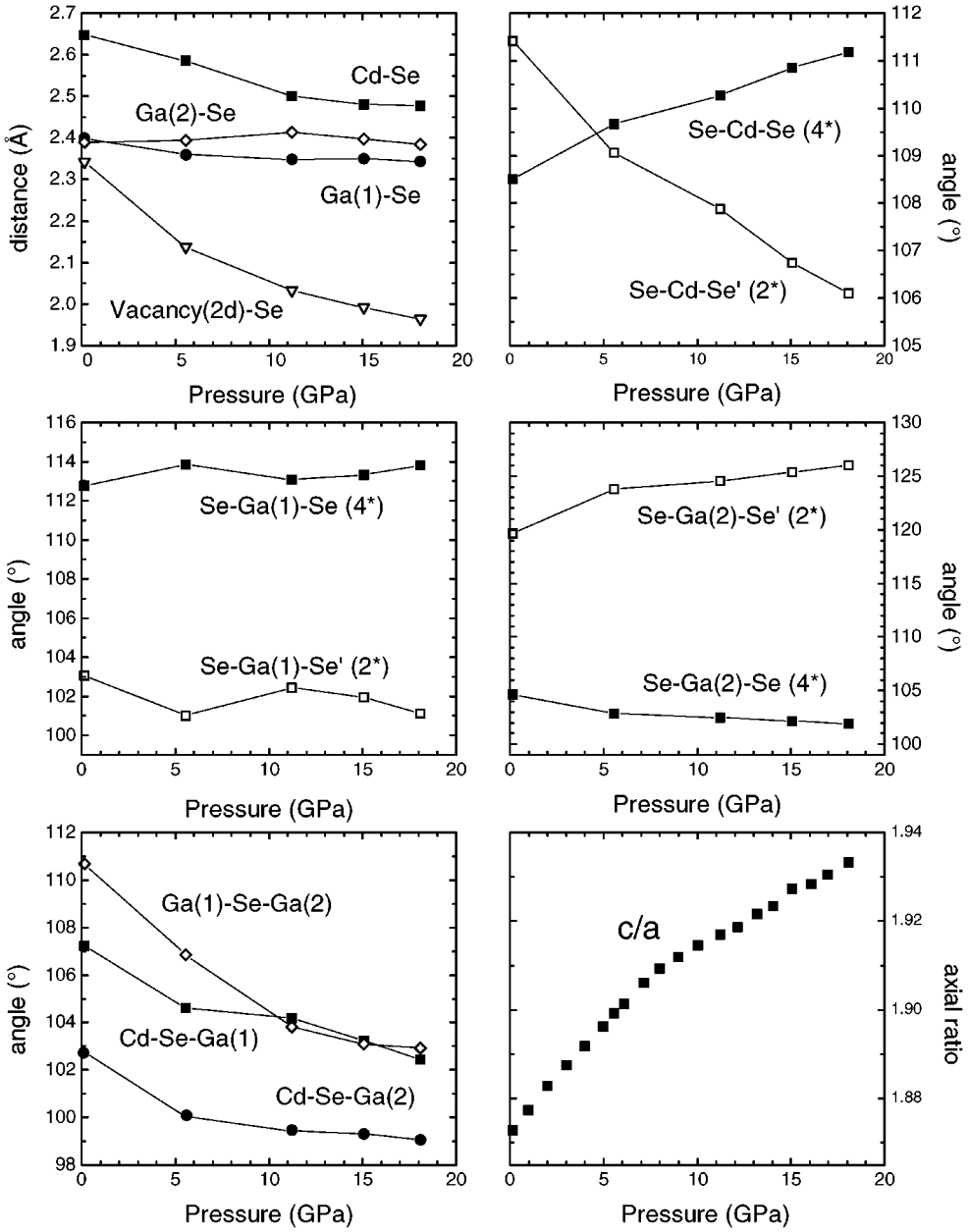

FIG. 4. Pressure dependence of structural parameters for $CdGa_2Se_4$ defect chalcopyrite ($I\bar{4}$, $Z = 2$). Representative estimated standard deviations for distances and angles are given in Table 1.

In the case presented here, it is apparent that δ approaches 0.05 at a pressures above 20 GPa ($\delta = 0.07$ at 18.1 GPa) where a new phase is formed (Fig. 2).

Figure 5 shows measured diagrams of the new phase at 28.8 GPa and of the ambient pressure phase obtained after decompression. The simulated pattern in the NaCl structure ($Fm\bar{3}m$, $Z = 4$) for the high pressure phase accounts very well for all the observed reflections and their intensities. The Se atoms are located at the 4*b* site (0.5, 0.5, 0.5), while both Cd and Ga atoms with fractional occupancy values of 0.25 and 0.5, respectively, are at the 2*a* site (0, 0, 0). The anomalous broadening of the reflections could be in part due to the strain in the sample at these pressure conditions. It could also result from the complete disorder of the cations and vacancies in the rock-salt structure. The peaks in the pattern of the fully decompressed sample (at atmospheric pressure) agree very well with the peaks in the simulated diagram of the corresponding zinc-blende structure ($F\bar{4}3m$, $Z = 4$), assuming that the Se atoms fully occupy the 4*c* site (0.25, 0.25, 0.25), while both Cd and Ga atoms with fractional

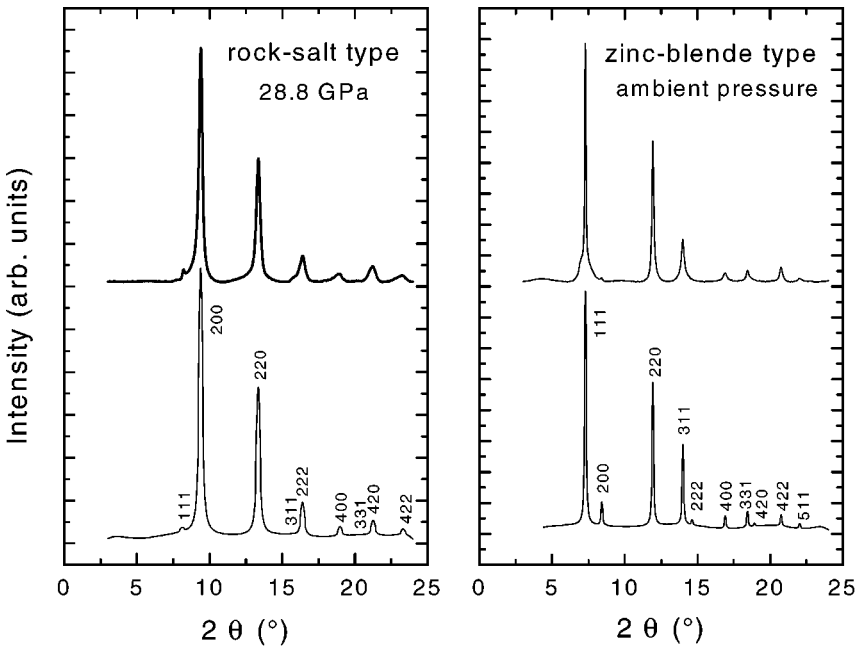

FIG. 5. Comparison of the measured diffractograms (top) with calculated patterns (bottom) for the disordered rock-salt ($Fm\bar{3}m$, $a = 5.03$ Å) and zinc-blende ($F\bar{4}3m$, $a = 5.64$ Å) structures of $CdGa_2Se_4$ at 28.8 GPa and at ambient pressure after decompression, respectively ($\lambda = 0.41416(1)$ Å). Backgrounds in the measured diffractograms are subtracted. Profile parameters for the calculated patterns were extracted from the measured diagrams using the program PowderCell (27).

occupancies of 0.25 and 0.5, respectively, reside at the 4*a* position (0, 0, 0). However, such a model cannot exactly account for the intensity of the (200) reflection. It also does not explain the anomalous shape of the (111) peak. The anomalous peak shape may indicate that the recovered material could largely be inhomogenous with defects and different disorder schemes at both the cation and anion sites.

The pressure dependence of lattice parameters and unit cell volumes for all the polymorphs of $CdGa_2Se_4$ is shown in Fig. 6. At the phase transition from defect chalcopyrite to rock-salt at 21.4 GPa, the relative volume change, taken for one formula unit, is $-6(1)\%$. The estimation of the volume change between $CdGa_2Se_4$ zinc-blende and rock-salt is complicated by the coexistence of the two phases in the intermediate pressure region and by possible inhomogenities. The cubic lattice parameter of the recovered sample ($F\bar{4}3m$, $Z = 4$) is smaller than the *a* lattice parameter of the defect chalcopyrite structure by 1%. The volume per formula unit, on the other hand, matches that of the starting phase, within the relatively large error margin of 0.8% (due to disorder effects) for the volume of the zinc-blende phase. We have fitted a Murnaghan-type pressure-volume relation to the experimental data for the chalcopyrite phase up to 7 GPa. The equation of state parameters (volume V_0, bulk modulus B_0 and pressure derivative B' of the bulk modulus, all taken at a reference pressure of zero) are $V_0 = 177.4(2)$ Å^3 (a half of the actual unit cell volume), $B_0 = 41.5(2)$ GPa, $B' = 5.0(1.0)$.

Optical Reflectivity

Figure 7 shows optical reflectance spectra of $CdGa_2Se_4$ measured at different pressures. The reflectance of the ambient pressure phase (at 2.4 and 14.9 GPa) is quite low due the reduced refractive index difference between sample and diamond (compared to a sample-air interface). The increase of the reflectance toward the UV range is attributed to the refractive index dispersion of the sample and the onset of direct interband transitions. Structure due to interband transitions is not resolved in these spectra. Optical reflectivity and absoption spectra at ambient pressure indicate a direct band gap of 2.57 eV for the present sample (23, 24).

The high pressure phase (spectra at 20.5 and 31.5 GPa) shows much enhanced values of the reflectance and in particular a Drude-like tail in the near-infrared spectral range. The latter feature indicates that the high pressure phase is metallic. The position of the Drude edge is not a direct measure of the carrier density, because screening effects due to interband transitions need to be taken into account in the analysis. To get a rough estimate of the carrier density, we have fitted a Drude–Lorentz oscillator model to the reflectance spectrum at 31 GPa, using expressions and following the approximate sum rule consider-

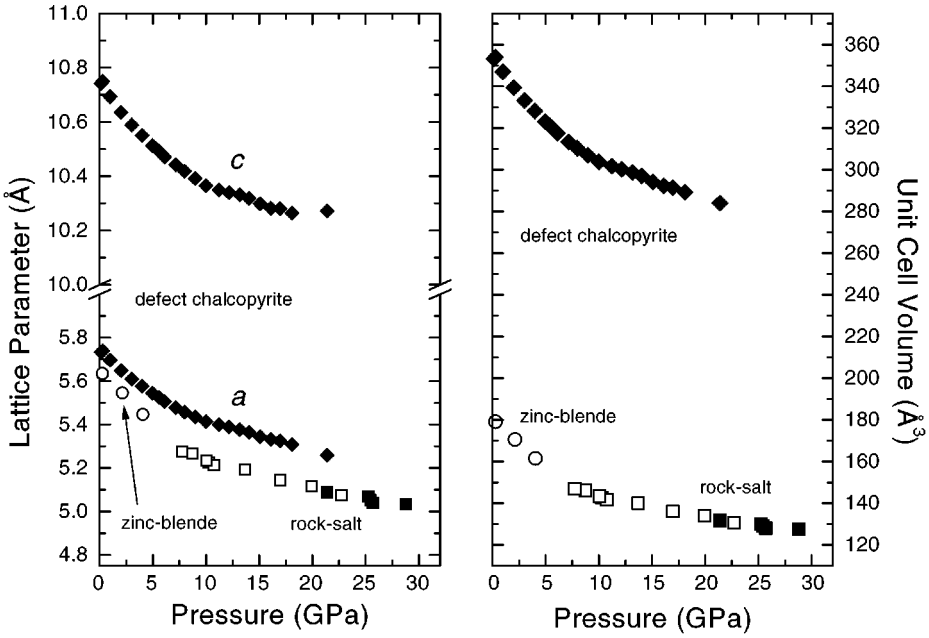

FIG. 6. Pressure dependence of lattice parameters and unit cell volumes for $CdGa_2Se_4$. Diamonds, squares, and circles represent the data points for the defect chalcopyrite ($I\bar{4}$), rock-salt ($Fm\bar{3}m$), and zinc-blende ($F\bar{4}3m$) structures, respectively. Refinement of lattice parameters for the coexisting rock-salt and zinc-blende phases at the pressure range 3–7.5 GPa was not attempted. Solid and open symbols stand for the data upon compression and decompression, respectively.

ations discussed in Ref. (18). The estimated carrier density, assuming an effective mass of one, is about $3 \times 10^{21}/\text{cm}^3$.

The reflectivity spectrum of the recovered sample does not show a Drude-like tail at the low-energy region, indicating that it is semiconducting. Furthermore, the reflectance spectrum is similar to that of the starting defect chalcopyrite phase at 2.4 GPa, indicating an overall similarity of the optical response.

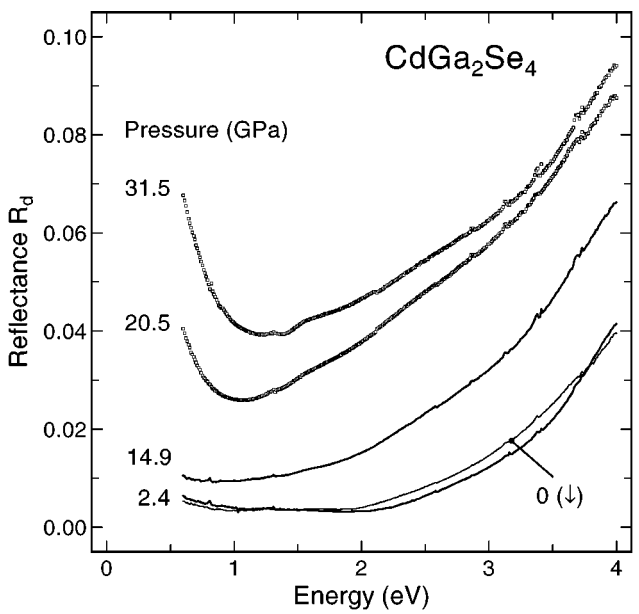

FIG. 7. Optical reflectivity spectra at different pressures. Spectra represented by thick lines and open symbols are for the defect chalcopyrite and rock-salt phases, respectively. The spectrum of the decompressed sample is shown as a thin line.

CONCLUSIONS

The results of this study demonstrate that cadmium selenogallate with the defect chalcopyrite structure transforms directly into the rock-salt structure, where the vacancy and all cations are completely disordered. There is no indication for the presence of any intermediate zinc-blende and/or rock-salt derived phases, similar to what has been experimentally observed for copper thiogallates and thioaluminates with the ideal chalcopyrite structure (6–8). The structural distortions in the defect chalcopyrite upon compression are due to the displacement of the anions toward the empty site, while the tetrahedra enclosing the void are tilted. The transformation to the disordered NaCl-type modification takes place when the factor $\delta = 2 - c/a$, the measure of a tetragonal distortion in zinc-blende superstructures, approaches values below 0.05 at pressures above 20 GPa. The complete disordering of the vacancy and cations in the sixfold-coordinated phase leads to metallic properties. Upon decompression, the high pressure phase is observed down to about 3–4 GPa. The recovered semiconducting sample is of the zinc-blende type, where the vacancy and all cations are fully disordered. The results of optical

reflectivity measurements, correlated with the structural details extracted from X-ray diffraction data, clearly demonstrate that disorder of vacancies and atoms at the cationic sublattice is not sufficient to induce metallic properties of the material. The metallic properties are observed only for the high pressure rock-salt structure with sixfold-coordinated atoms, but not for the tetrahedral zinc-blende type.

The present observations are different from previous observations that were based entirely on the results of Raman scattering measurements (15). Here we find no evidence for the formation of the disordered NaCl phase at 15 GPa in two stages with defect famatinite and zinc-blende intermediates, occurring at 5.5 GPa and 11.0 GPa, respectively. The recovered sample is not a disordered rock-salt structure either. A possible explanation could be that the spectroscopic technique is not sufficient to probe structural phase transitions. This discrepancy could also be rationalized by the complexity of the pressure-induced processes that depend on the rate of pressure increase or decrease, or more general, on the pressure dependence of the potential barriers between different low- and high-pressure phases with different degrees of disorder. During a fast decompression, the metastable rock-salt structure is recovered to ambient conditions (15). However, when the sample is decompressed slowly, as it was in this study, a disordered zinc-blende structure is obtained. It should be recalled that $CdIn_2Se_4$, $CdIn_2Te_4$, and $HgIn_2Te_4$, all with the cadmium thiogallate structure at ambient conditions, transform into the NaCl type at high pressures and high temperatures, while the recovered samples are of the zinc-blende type (25, 26). Our study shows that the final decompressed thiogallate product would depend on the rate of pressure release at room temperature.

ACKNOWLEDGMENT

V.V.U. acknowledges financial support from Deutscher Akademischer Austauschdienst.

REFERENCES

1. A. F. Wells, "Structural Inorganic Chemistry," 5th ed. Clarendon Press, oxford, 1984.
2. V. Krämer, B. Frick, and D. Siebert, *Z. Kristallogr.* **165,** 151 (1983).
3. V. Krämer, D. Siebert, and S. Febbraro, *Z. Kristallogr.* **169,** 283 (1984).
4. C. K. Lowema and T. A. Vanderah, *Acta Crystallogr. Sect C: Cryst. Struct. Commun.* **47,** 919 (1991).
5. T. Hanada, F. Izumi, Y. Nakamura, O. Nittono, Q. Huang, and A. Santoro, *Physica B* **241,** 373 (1997).
6. C. Carlone, D. Olego, A. Jayaraman, and M. Cardona, *Phys. Rev. B* **22,** 3877 (1980).
7. A. Werner, H. D. Hochheimer, and A. Jayaraman, *Phys. Rev. B* **23,** 3836 (1981).
8. J. P. Itié, V. Brois, D. Martinez-Garcia, A. Polian, and A. San-Miguel, *Phys. Status Solidi B* **211,** 323 (1999).
9. L. Roa, J. González, J. C. Chervin, and A. Chevy, *Phys. Status Solidi B* **211,** 429 (1999).
10. L. Roa, J. C. Chervin, J. P. Itié, A. Polian, M. Gauthier, and A. Chevy, *Phys. Status Solidi B* **211**, 455 (1999).
11. H. K. Eba, N. Ishizawa, F. Marumo, and Y. Noda, *Phys. Rev. B* **61,** 3310 (2000).
12. Y. Mori, S. I. Iwamoto, K. I. Takarabe, S. Minomura, and A. L. Ruoff, *Phys. Status Solidi B* **211,** 469 (1999).
13. K. J. Range, G. Engert, and A. Weiss, *Solid State Commun.* **7,** 1749 (1969).
14. A. Jayaraman, P. D. Dernier, H. M. Kasper, and R. G. Maines, *High Temp. High Pressure* **9,** 97 (1977).
15. V. V. Ursaki, I. I. Burlakov, I. M. Tiginyanu, Y. S. Raptis, E. Anastassakis, and A. Anedda, *Phys. Rev. B* **59,** 257 (1999).
16. W. R. L. Lambrecht and S. N. Rashkeev, *Phys. Status Solidi B* **217,** 599 (2000); S. I. Radautsan, I. M. Tiginyanu, *Jpn. J. Appl. Phys. Suppl.* **32-3,** 5 (1993); G. C. Bhar, *Jpn. J. Appl. Phys., Suppl.* **32-3**, 653 (1993).
17. A. P. Hammersley, S. O. Svensson, M. Hanfland, A. N. Fitch, and D. Häusermann, *High Pressure Res.* **14,** 235 (1996).
18. A. R. Goñi and K. Syassen, *in* "Semiconductors and Semimetals," Vol. 54, p. 247. Academic Press, New York, 1998.
19. H. K. Mao, J. Xu, and P. M. Bell, *J. Geophys. Res.* **91,** 4673 (1986).
20. A. C. Larson and R. B. von Dreele, "GSAS: General Structure Analysis System," Los Alamos National Laboratory, 2000.
21. P. W. Stephens, *J. Appl. Crystallogr.* **32,** 281 (1999).
22. J. J. M. Binsma, L. J. Giling, and J. Bloem, *Phys. Status Solidi A* **63,** 595 (1981).
23. N. N. Syrbu and V. E. Tezlevan, *Physica B* **210,** 43 (1995).
24. R. Bacewicz, R. Trykozko, A. Borghesi, M. Cambiagi, and E. Reguzzoni, *Phys. Lett. A* **75,** 121 (1979).
25. K. J. Range, W. Becker, and A. Weiss, *Z. Naturforsch.* **23b,** 1261 (1968).
26. K. J. Range, W. Becker, and A. Weiss, *Z. Naturforsch.* **24b,** 1654 (1969).
27. W. Kraus and G. Nolze, *CPD Newsletter*, No. 20, International Union of Crystallography, 1998.